Star poly(lactide-co-glycolide) and poly(ϵ-caprolactone) polyurethanes with shape memory properties for biomedical applications

Gaëlle Savin, Iliass Kadmiri, Sylvain Caillol, Philippe Gonzalez, Aurélien Lebrun, Michel Assor, Ghislain David, Benjamin Nottelet

European Polymer Journal 220 (2024) 113442

Contents lists available at ScienceDirect

European Polymer Journal

journal homepage: www.elsevier.com/locate/europolj

Star poly(lactide-co-glycolide) and poly(ε-caprolactone) polyurethanes with shape memory properties for biomedical applications

Gaëlle Savin [a,b,c], Iliass Kadmiri [c], Sylvain Caillol [a], Philippe Gonzalez [c], Aurélien Lebrun [d], Michel Assor [b], Ghislain David [a], Benjamin Nottelet [c,e,*]

[a] ICGM, Univ Montpellier, CNRS, ENSCM, Montpellier, France
[b] Arthrocart Biotech, Marseille, France
[c] IBMM, Univ Montpellier, CNRS, ENSCM, Montpellier, France
[d] LMP, Univ Montpellier, CNRS, ENSCM, Montpellier, France
[e] Department of Pharmacy, Nîmes University Hospital, Univ Montpellier, Nimes, France

ARTICLE INFO

Keywords:
Poly(ester-urethane) foam
Star-PLGA
Resorbable porous matrix
Shape memory
Flexural strength

ABSTRACT

Shape memory polyurethane (SMPU) have the capacity to alter and regain their form in reaction to a stimulus (*eg.* temperature, pH) and have been investigated in biomedical applications. In this work, the shape memory properties of poly(ester-urethane)s (PEU) are studied as a function of the functionality of the poly(lactide-co-glycolide) (PLGA) and poly(e-caprolactone) (PCL) pre-polymers. Two distinct series of PEU are synthesized by reaction between linear and star-shaped PLGA polyols initiated by pentaerythritol (4-arms PLGA) or dipentaerythritol (6-arms PLGA) with PCL di-isocyanate prepolymers. The different PEUs exhibit thermally actuated shape memory properties and tunable mechanical properties with Young's moduli reaching up to 96 MPa and elongation at break reaching 930 %. The integration of low amounts of PLGA star within the PEU structure increases the material's shape memory properties, enhancing both fixity (from 45 % to 96 %) and recovery ratios (from 88 % to 92 %). Further exploration into potential applications led to the formulation of porous foams *via* the solvent casting/particles leaching (SC/PL) process. These foams exhibited high porosity ranging from 74 % to 83 % with pore sizes spanning from 100 to 300 μm. Their mechanical properties are close to the human meniscus with Young's modulus ranging from 0.13 MPa to 0.53 MPa. Moreover, integration of PLGA star within the PEU scaffold decreases the flexural strength that is an important parameter for potential mini-invasive surgery.

1. Introduction

Biomedical engineering challenges lean on research in materials with specific thermal and mechanical properties that can be processed into defined shapes and geometries. Shape memory polymers (SMPs) have the specific ability to alter and regain their shape in response to various stimuli (like temperature and pH) and have been investigated in biomedical applications. [1,2] This class of polymer rose interest for clinician as these materials can undergo geometric changes after device implantation in human body. SMPs find therefore applications in minimally invasive surgical procedures to reduce contamination risk and hospital stay. In addition to their biocompatibility, SMPs can be designed to present various actuation temperature, strain recovery, stress relief, or moduli under physiological conditions. Many SMP systems exhibit tunability of these properties, due to their crosslinked nature and degree of crosslinked interconnectivity [3]. Among SMPs, shape memory polyurethanes (SMPUs) have been investigated in biomedical applications by various researchers [2,4–9] due to their high toughness (resulting from interchain hydrogen bonding between urethane linkage) and due to their hard segment (HS) that play an important role in recovering the material's permanent shape [10,11]. Moreover, poly(ester-urethane)s (PEU) exhibit excellent physical and mechanical properties, tunable degradation rate and good biocompatibility. [4,7–9] Indeed, SMPU can be characterized as ideal material for medical devices due to their ability to keep a specific shape during surgery, or delivery, and to recover their original shape afterwards in human body at physiological temperature (37 °C) and pH (7.4) [12]. For example, Veloso-Fernandez et al [9]. worked on a new generation of biocompatible SMPUs, from poly(tetramethylene glycol) (PTMG), hexamethylene diisocyanate (HDI), and castor oil or butanediol (BDO) or

* Corresponding author at: IBMM, Univ Montpellier, CNRS, ENSCM, Montpellier, France.
E-mail address: benjamin.nottelet@umontpellier.fr (B. Nottelet).

https://doi.org/10.1016/j.eurpolymj.2024.113442
Received 28 June 2024; Received in revised form 2 September 2024; Accepted 3 September 2024
Available online 12 September 2024

mixture of both, as chain extenders, without catalyst nor solvent. They evaluated the shape memory behavior with thermo-mechanical cycles measured by thermomechanical analysis (TMA) to determine the deformation (R_d), fixity (R_f) and recovery (R_r) ratios and found strain values between 7 and 8 %, R_f above 80 %, and R_r above 90 %. However, strain values below 10 % are quite low to fully demonstrate the shape memory capacity. The work of Baek [4] evaluated the shape memory properties of SMPUs synthetized with two different aliphatic isocyanates (HDI and isophorone diisocyanate (IPDI)). The sample with 80 mol% IPDI content showed the best SM properties with stable R_d, R_f and R_r values around 70 %, 98 % and 99 %, respectively. They showed the thermoplastic behavior by the transcarbamoylation reaction. On their side, Luo et al. [13] developed two biodegradable SMPUs from dicyclohexylmethane-4,4′-diisocyanate (HDMI), PCL with two different chain extenders: BDO and 5,50,6,60-tetrahydroxy-3,3,30,30-tetramethyl-1,10-spirobisindane (TTSBI), a molecule reported to be an antioxidant. Both PU exhibited fixity ratios between 91 and 99 %, and recovery ratios between 85 and 98 % with excellent strain of 200 %.

Besides medical devices, SMPUs are being investigated in the field of tissue engineering. Shaabani et al. [7] reported a conducting self-healing scaffold with shape memory properties for bone tissue engineering applications. They synthetized a PU from PCL, IPDI, and cystamine (CYS) or hexamethylenediamine (HMDA) with disulfide and gold-thiol bond. Bending test was performed to evaluate shape recovery ($R_r = 95$ %) and fixity ($R_f = 96$ %), with a fast shape recovery at physiological temperature. Ramezani et al. [8] investigated the influence of HS and soft segment (SS) on the shape memory behaviour of HDI, polypropylene glycol (PPG), and triethylene glycol-based SMPU. The materials showed R_f between 72 and 76 % and R_r between 91 and 94 %, cytocompatibility and cells attachment. SMPUs are also good candidates for bone tissue engineering where the can fill bone defects and promote bone formation. Wang et al. [14] investigated enhanced mechanical properties of SMPU using extended diisocyanates based on HDI and isosorbide (ISO) (HDI-ISO-HDI and HDI-ISO-HDI-ISO-HDI) for the HS, and PDLLA as the SS. The materials reached 99.8 % fixity ratio, 90.2 % of recovery ratio and a 50 % strain. Bil et al. [15] designed electrospun SMPUs for self-fitting tissue engineering grafts and drug delivery systems. They investigated the SM of 2 types of PU: PU-PLGA and PU-PLLA/PEG, differing in SS composition (PLGA, PEG and PCL with various molecular weights). The materials exhibited fixity ratios ranging from 78 to 99 %, recovery ratios from 90 to 99 %, and 100 % strain. They selected PU based on PCL, PLGA, BDO and HDI as a result of their better SM performance. Hong et al. [16] focused on tissue-regenerative biomaterials based on PCL-PU copolymers with hyperelasticity (from 800 to 1,600 % elongation), SM and cell adhesion properties. PU materials were synthetized in a one-step polymerization reaction from PCL diol, HDI and isosorbide derivatives (ethoxylated isosorbide, propoxylated isosorbide and bare isosorbide). The SM effect was investigated on different processed objects (film, thread and 3D scaffolds) and showed recovery ratios ranging from 40 to 80 % (in tension or compression mode), and fixity ratios from 40 to 95 %.

To summarize, different SMPU have been investigated, based on aliphatic isocyanates (HDI, IPDI) and different diols including poly(D,L-lactic acid) (PDLLA), polypropylene glycol (PPG), poly(ε-caprolactone) (PCL), triethylene glycol, glycerol, castor oil. However, for PLGA, PCL based PEU, the influence of the polyol functionality on the shape memory properties has never been explored to the best of our knowledge [4,7–9].

In our previous work, we designed a thermoplastic PEU in two steps using HDI functionalized prepolymer PCL di-NCO and PLGA di-OH as chain extender [17]. The focus of the present work is to investigate the shape memory ability of a library of bioresorbable PEUs synthetized from PLGA, star PLGA, and PCL acting as soft segments combined with HDI acting as HS.

First, PLGAs with functionalities of two, four and six are synthetized by ring opening polymerization using 1,3 propanediol, pentaerythritol and dipentaerythritol as initiators, respectively, before thorough NMR (^{13}C and ^{1}H) investigations to analyze their chain ends and allow efficient polyadditions.

Secondly, PEUs are synthetized via a two-step process. PCL diol ($M_n = 2{,}000$ g mol^{-1}) is functionalized from an excess of HDI to form a PCL di-NCO prepolymer. A library of different PEUs is obtained by polyaddition between PCL di-NCO and star PLGA/ linear PLGA diol at various ratios to investigate the effects of PGLA functionality on the mechanical, thermal and degradation properties. The resulting PEUs are first processed into films to analyze their shape memory ability. Finally, the PEUs fully soluble in THF were selected to form porous structure by a solvent casting/particles leaching (SC/PL) process. Their mechanical and thermal properties, pore size, porosity, and flexibility are evaluated to study their possible applications in meniscus repair.

2. Experimental procedure

2.1. Materials

D,L-lactide and glycolide were purchased from Corbion (Gorinchem, The Netherlands). Tin (II) 2-ethylhexanoate (92.5–100 %), poly(ε-caprolactone) diol (PCL, $M_n = 2{,}000$ g mol^{-1}), 1,3-propanediol (>98 %), pentaerythritol and dipentaerythritol were provided by Sigma Aldrich (St-Quentin Fallavier, France) and used as received. 1,4-Dioxane (ACS-Reagent), distilled in the presence of CaH_2, was provided by Honeywell (Offenbach, Germany). Diethyl ether, n-pentane, dichloromethane and sodium chloride were provided by Carlo Erba Reagents (Val de Reuil, France). Hexamethylene diisocyanate (HDI; >98 %) was provided by TCI Europe (Zwikndrecht, Belgium) and used as received.

2.2. Methods

2.2.1. Nuclear magnetic resonance (NMR)

All ^{1}H NMR were done on a Bruker Avance III HD 400 MHz NMR equipped with BroadBand Inverse (BBI) probe. ^{1}H and 2D NMR spectra were recorded at 298 K on Bruker Avance III 600 MHz NMR spectrometer using TCI Cryoprobe Prodigy®. 2D homonuclear ^{1}H–^{1}H g-COSY (1 scan, 256 real (t1) × 2048 (t2) complex data points) and 2D heteronuclear spectra ^{13}C–^{1}H g-edited HSQC (2 scans, 256 real (t1) × 2048 (t2) complex data points) were acquired to assign the compound. Quantitative ^{13}C NMR spectra were recorded at 298 K on a Bruker AVANCE III 500 MHz NMR spectrometer equipped with a 5 mm 1H/X BBO Helium cryoprobe and on Bruker Avance III 600 MHz NMR. 1D-sequence with inverse gated decoupling was used with a relaxation delay of 30 s and 256 scans. All Chemical shift are given in δ ppm calibrated with residual protic solvent (*e.g.* $CDCl_3$: 7.26 ppm -^{1}H / 77.16 ppm – ^{13}C). Spectra were processed and visualized with Topspin 3.6.2 (Bruker Biospin) on a Linux station for 2D spectra and with Mestrenova software 14.2.1 for 1D spectra.

2.2.2. Fourier transform infrared (FTIR)

The Fourier transform infrared (FTIR) spectra were recorded using attenuated total reflection (ATR) in transmission mode with a Thermo-Scientific Nicolet iS50 FT-IR Flex Gold spectrometer equipped with a deuterated triglycine sulfate (DTGS) detector. The characteristic IR absorption bands are reported in cm^{-1}. Data from FTIR are used in macros linked to the machine software (OMNIC) to monitor the progress of the reaction based on the variation (reduction) of the isocyanate peak, using Eq. (1), where N_0 is the total area of the isocyanate peak at t_0, and N is the final area at the end of the reaction.

$$\text{Conversion}\,(\%) = \frac{N_0 - N}{N_0} \times 100 \quad (1)$$

2.2.3. Thermogravimetric analyses (TGA)

Thermogravimetric analyses of PEU were performed on a Netzsch

STA 449 F1 TGA under 50 mL.min^{-1} argon. The protective gas used was argon with a 20 mL.min^{-1} flow. Approximately 10 mg of sample was placed in an alumina crucible and heated from room temperature to 800 °C with a 20 °C.min^{-1} heating ramp.

2.2.4. Differential scanning calorimetry (DSC)

Differential scanning calorimetry analyses were carried out using a NETZSCH DSC200F3 calorimeter. Constant calibration was performed using indium, n-octadecane, n-octane, adamantane, biphenyl, tin, bismuth and zinc standard. Nitrogen was used as the purge gas at 40 mL.min^{-1}. Approximately 10 mg of sample was placed in pierced aluminum pans and the thermal properties were recorded between − 150 °C and 200 °C at 20 °C.min^{-1} to observe the T_g. Glass transition temperatures were measured on the second heating ramp to erase the thermal history of the polymer.

2.2.5. Isocyanate equivalent weight (IEW) and hydroxyl equivalent weight (HEW)

The IEW and HEW of HDI and PLGA respectively, were determined by ^{1}H NMR titration, using benzophenone as the internal standard. For each compound, three samples were prepared with approximately 50 mg of the sample and 20 mg of benzophenone dissolved in 0.5 mL of $CdCl_3$ and analyzed by ^{1}H NMR. The IEW was determined by integration of the signals at 3.30 ppm for HDI and 7.5 ppm for benzophenone (HDI IEW=79 g eq^{-1}). An example is given for the IEW calculation of PCL functionalized with HDI (prepolymer), in Eq. (2), where $N_{H\ eq\ PCL\text{-}HDI}$ corresponds to the number of hydrogens in alpha to the hydroxyl moiety.

$$\mathrm{IEW\,(PCLdi-NCO)} = \frac{m_{PCL-HDI} \times \mathrm{N_{H\,eq\,PCL-HDI}} \times \int_{7.28}^{7.87} benzophenone}{m_{benzophenone} \times \mathrm{N_{N\,eq\,benzophenone}} \times \int_{3.31}^{3.56} PCLdi-NCO} \quad (2)$$

2.2.6. Size exclusion chromatography multi angle light scattering (SEC-MALS)

SEC-MALS measurements were performed on Agilent 1260 Infinity triple detection SEC set-up comprising a Wyatt Optilab MALS detector, and an Agilent differential refractometer. Separation was achieved using 2 PLgel mixed B LS columns (7.5 mm × 300 mm). The eluent was tetrahydrofuran (THF) at 30 °C at a flow rate of 1 mL.min^{-1}. The refractive index increment (dn/dc) of PLGA, PCL, the prepolymer and the PEU was obtained as follows. Five different concentrations (0.25 mg.mL^{-1}, 0.5 mg.mL^{-1}, 0.75 mg.mL^{-1}, 1 mg.mL^{-1}, 1.5 mg.mL^{-1}, 2 mg.mL^{-1}) of the polymer in THF were injected and the resulting RI signals were plotted as a function of concentration. The dn/dc values of the polymers are given in Table S1 and were used for the MALS analysis of all samples in this work.

2.2.7. Gel fraction

PEUs samples (around 50 mg) were immersed in THF (3 mL) for 24 h under stirring at room temperature. After 24 h, the solvent was removed and PEUs were dried under vacuum at 40 °C for 24 h. The gel fraction (GF) was calculated using Eq. (3), where m_d is the mass of the dried material, and m_0 the initial mass. GF values are given as mean of triplicates.

$$\mathrm{GF} = \frac{m_d}{m_0} * 100 \quad (3)$$

2.2.8. Scanning electron microscopy (SEM)

A scanning electron microscope (Phenom ProX Desktop) was employed to observe the porous structure of the polyurethane scaffolds. Cubic samples (2–3 mm per side) were analyzed. The cross sections of the samples were sputter coated with gold. SEM observation was carried out at 10 kV. The average pore size and analysis of pore size distribution in the samples were determined with ImageJ program. Pore sizes are expressed as mean +/- SD ($n = 60$).

2.2.9. Hot press processing

Presse Carver 3,690 was employed to create polyurethane-based film. The PEU was dried at 40 °C for 24 h to remove trapped solvents, and then ground into powders to achieve more homogeneous films. The process was conducted under these conditions: a temperature of 120 °C was chosen based on preliminary thermal analysis (TGA, DSC) and optimization studies. The pressure was maintained at 1.2 tons to ensure proper bonding and material densification. The specimens were exposed to these conditions for 20 min, facilitating adequate heat transfer and molecular rearrangement within the material. All the films were left at room temperature for 3 days to allow the recrystallisation of PCL before conducting the uniaxial tensile test and DMA tests.

2.2.10. Tensile, compression, and three-point bending tests

Cubic samples (10 mm per side) were cut for testing. Compressive strengths at 20 % of deformation and Young's moduli were determined using Instron tester model equipped with 100 N load cells. The measurements were carried out at a crosshead speed of 5 mm.min^{-1}. All given values are given as means of three measurements +/- SD. The compression modulus was determined via the stress–strain curve of the material.

Tensile tests were performed at room temperature on at least three different dog-bone specimens of ≈ 2 mm width, 14 mm gauge length, and ≈ 2 mm thickness. All tensile tests were performed with an Instron 5900 machine at a deformation rate of 10 mm.min^{-1}.

Test bars of dimensions 9x8x50 mm (thickness x width x length) were tested in three-point bend cell with a crosshead displacement of 5 mm.min^{-1} at 100 % of deformation. The span length was 19 mm. The Young's modulus was calculated from the slope of linear region of the curve. The flexural modulus was calculated with the slope of the flexural strain stress curve.

The flexural strength was calculated using Eq. (4), with F_{max} the maximum force at 100 % flexion, l length of the sample, t thickness and w width:

$$\mathrm{Flexural\ strenght} = \frac{3*F_{max}*l}{2*t^2*w} \quad (4)$$

2.2.11. Dynamic mechanical analyses (DMA)

Dynamic Mechanical Analyses (DMA) were carried out on a Mettler DMA instrument with STARe software.

Dynamic Mechanical Analyses (DMA) were performed to investigate the viscoelastic properties of the synthetized foams and PU films through the storage modulus (E'), the loss modulus (E'') and loss tangent (tan δ) measurement. E' and E'' are expressed in MPa and tan δ is dimensionless, calculated as seen in Eq. (5). Experiments were carried out on a Mettler Toledo DMA 1 Star instrument with STARe software. T_α was obtained as the temperature for which value of E'' was maximum, or tan δ if the peak of E'' was not clear.

$$\tan\delta = \frac{E'}{E''} \quad (5)$$

- *Traction mode*

PU films were cut into rectangular film (7x4x3 mm^3) and mounted on a tensile test clamp. Experiments were conducted from while heating at a rate of 2 °C/min from 10 °C to 60 °C at a frequency of 1 Hz with a fixed displacement of 10 μm and a preload of 1 N.

- *Compression mode*

Compression of cubic samples (2x2x2 mm^3) was performed while

heating at a rate of 2 °C/min from −40 °C to 60 °C, keeping the frequency at 1 Hz.

2.2.12. Thermo-mechanical analysis (TMA)

Thermo-mechanical analysis (TMA) was performed on a Mettler DMA instrument in tensile mode to evaluate the shape memory behavior of the different PEUs film and foams.

PEU films were cut into rectangular samples (1x5x1 mm^3) and PEU foams were cut into cubic shapes. Samples were heated above the T_α, previously measured by DMA. A force of 2 N was applied for PEU films. After 5 min, the maximum strain can be obtained (ε_m). The sample was cooled quickly below its T_α to fix the temporary shape (ε_t). The force was removed and the sample was kept at this temperature during 10 min. During the recovery step, the PEU was reheated above its T_α to recover its permanent shape (ε_p). This method allows the calculation of the following characteristic ratios: the deformation ratio (R_d), the fixity ratio (R_f) and the recovery ratio (R_r), with L the initial length of the sample (L=1 mm), as illustrated in Eq. (6), Eq. (7) and Eq. (8).

$$R_d\,(\%) = \frac{\varepsilon_m}{L} \times 100 \tag{6}$$

$$R_f\,(\%) = \frac{\varepsilon_t}{\varepsilon_m} \times 100 \tag{7}$$

$$R_r\,(\%) = \frac{\varepsilon_p}{L} \times 100 \tag{8}$$

2.2.13. PLGA synthesis

PLGA was obtained via the ring opening polymerization (ROP) of lactide and glycolide with stannous octoate $Sn(Oct)_2$ initiated with 1,3-propanediol, pentaerythritol or dipentaerythritol. D,L-lactide and glycolide were dried under vacuum overnight prior to use.

Equimolar D,L-lactide and glycolide were charged into a rigorously dried 100 ml flask at T=130 °C under nitrogen flow. After observing a clear melt of monomers, the initiator was added, and 0.5 % of equivalent number relative to the initiator alcohol was introduced. The reaction was allowed to proceed for 3 h at 130 °C. After cooling to room temperature, the products were dissolved in 50 mL of THF and then precipitated in 500 mL of cold heptane. The polymer was collected by filtration and dried at 25 °C under vacuum for 24 h. The polymerization yield after precipitation was 90 %, 87 %, and 83 %, for PLGA2, PLGA4 and PLGA6, respectively. The quantities of monomers and initiators are indicated in Table S2. Full characterization of the PLGA2 can be found in our recent paper.[17] For the PLGA2 batch used in this work Mn = 1,900 g/mol. HEW were calculated using NMR analyses by comparison of the integrals of the signals of the initiator and of the glycolic/lactic units (see discussion for further details).

^{1}H NMR PLGA4 (400 MHz, $CDCl_3$, δ): 5.2 (m, 17H, H_c), 4.8 (m, 39H, H_b), 4.3 (m, 2H, $H_{c'}$), 4.2 (s, 4H, $H_{b'}$), 4.1 (m, 12H, H_a), 3.2 (m, 4H, H_f), 1.5 (m, 40H, H_d); HEW value = 933 ± 14 g eq^{-1}.

^{1}H NMR PLGA6 (400 MHz, $CDCl_3$, δ): 5.2 (m, 9H, H_c), 4.8 (m, 23H, H_b), 4.3 (m, 3H, $H_{c'}$), 4.2 (s, 4H, $H_{b'}$), 4.1 (m, 8H, H_a), 1.5 (m, 86H, H_d); HEW value = 385 ± 6 g eq^{-1}.

2.2.14. Poly(ester-urethane) synthesis

PCL-diol was end-capped with an excess of HDI at 80 °C, as previously described to form the prepolymer PCL di-NCO [17]. The extension of this prepolymer with PLGA was performed in a reactor. Linear (PLGA2) and star PLGA (PLGA4 and PLGA6) with different weight ratios (See Table S3) were added into a dry glass reactor flushed with nitrogen, with 17 mL of distilled dioxane. The reactor was heated to 100 °C, and 6 g of PCL di-NCO prepolymer was added, with 3 drops of tin(II) 2-ethylhexanoate. The system was reacted with a mechanical stirring blade (220 rpm) for different durations of time (depending on the formulation and gelation point), until the disappearance of isocyanate band at 2,300 cm^{-1}. Following the polyaddition, dioxane was slowly added to control the viscosity of the mixture and allow the transfer and use of the PEU. The polymer was then purified by precipitation in 80:20 diethylether: ethanol.

Table S3 gathers the quantities of prepolymers, and the values of hydroxyl equivalent weight (HEW) and isocyanate equivalent weight (IEW) used in the synthesis of the polyurethanes. For the sake of simplicity, we will adopt the following nomenclature: Cr-PEU-XY, where: Cr: represents the crosslinking nods of the PEU, X gives information on the proportion of star PLGA used, ranging from 5 to 15 %, the complement to reach 100 % being done with linear PLGA. Y provides insight into the initiator's nature employed for crosslinking, with 'P' for pentaerythritol, and 'D' for dipentaerythritol.

2.2.15. Foams preparation

Porous polymer scaffolds were prepared by SC/PL with NaCl salt as porogen agent. Briefly, 3 g of PEU was dissolved in 9 mL of THF and 15 g of NaCl crystals (sieved to 100–300 μm) were added to the polymer solution. After a vigorous mixing, the suspension was poured into a mould, rapidly frozen by immersion into liquid nitrogen before evaporation of the solvent at room temperature overnight. The foam was washed in distilled water at room temperature until clearance of salt crystals.

To characterize the foam, the porosity was calculated according to Eq. (9), where m is the mass of the foam (g), V the volume of the foam (cm^3), and ρ_{PEU} the volumic mass of the PEU (g/cm^3). Porosity values are the mean of three measurements +/- SD.

$$P = 1 - \frac{m}{\rho_{PEU} V} \times 100 \tag{9}$$

2.2.16. In vitro degradation

The kinetic of degradation was studied *in vitro* in standard conditions using phosphate buffer solution (PBS, pH=7.4) and in accelerated conditions using HCl aqueous solution (0.1 M, pH=1) at constant temperature (37 °C) and under continuous stirring (100 rpm). Foam samples were cut into cubic shape, weighted ($w_{dry,\,t0}$) and incubated in 1 mL media solution. The samples were removed from the medium at specific time points, washed with distilled water, carefully wiped and then dried to constant weight ($w_{dry,t}$). Degradation was monitored by determination of the weight loss and molecular weight decrease of the PEU. The remaining weight was calculated from Eq. (10).

$$\text{remaining mass}\,(\%) = \left(\frac{w_{dry,t}}{w_{dry,t0}}\right) \times 100 \tag{10}$$

3. Results and discussion

3.1. Star PLGA synthesis and characterization

PLGA was synthesized by ROP of an equimolar ratio of D,L-lactide and glycolide initiated by propanediol (see our previous work for NMR characterization [17]), dipentaerythritol (Fig. 1A), or pentaerythritol (Fig. 1B).

^{1}H NMR spectrum allowed us to determine the average molecular weight. For the PLGA spectra, the peaks H_c (at 5.22 ppm) and H_d (at 1.58 ppm), were attributed to the methine and methyl groups respectively of lactic units, and the peak b at 4.81 ppm was attributed to the methylene of glycolic units. PLGA chains can be either terminated by lactic acid or glycolic acid. Indeed, the analysis of the hydrogens in alpha position of the hydroxyl function ($H_{b'}$ and $H_{c'}$) is essential to calculate the HEW. However, due to the overlapping of those signals, ^{1}H NMR could not inform us on a precise integration. To fully assign the other signals and understand the functionality of the polymers, complementary 2D NMR analyses were therefore conducted. The objective was to obtain the integration of the hydrogens in alpha position of the hydroxyl function: $H_{b'}$ and $H_{c'}$.

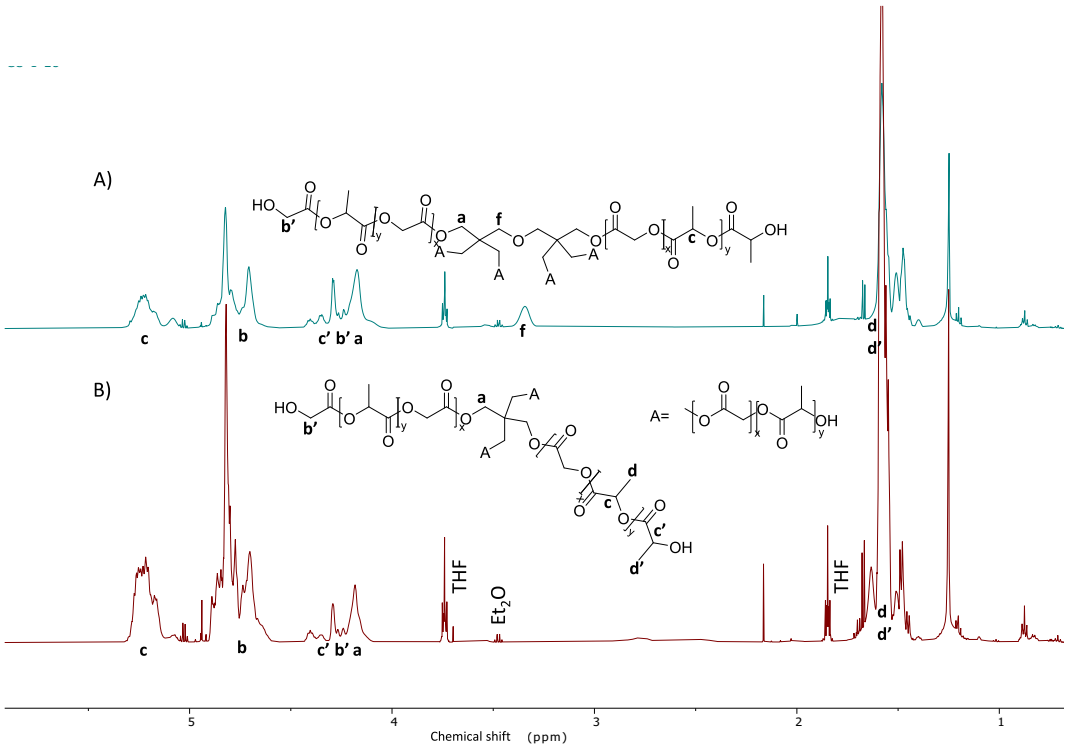

Fig. 1. ^{1}H NMR (600 MHz, $CDCl_3$) spectrum of A) 6-arms star PLGA (PLGA6) initiated with dipentaerythritol, B) 4-arms star PLGA (PLGA4) initiated with pentaerythritol.

As seen on HSQC spectrum in Fig. S1, red marks at 66.9 ppm and at 62.2 ppm were identified as $C_{c'}$ and C_c, respectively. In quantitative ^{13}C spectrum (Fig. S2), C_a, carbon at the core of the polymer, was integrated as 4 carbons as a reference, which could allow us to obtain the integration of the methine terminated group, $C_{c'}$ of 2.3. $H_{b'}$ was then determined by subtracting $H_{c'}$ (2.3H) and H_a (8H) to 14H (the integration of the signal gathering H_a, $H_{b'}$ and $H_{c'}$). In conclusion, $AH_{b'}$=3.7H and $AH_{c'}$=2.3H.

In a second step, the average hydrogen in alpha position of the hydroxyl function was obtained by the ratio of integration of LA (%LA) and GA (%GA) and their corresponding hydrogens in alpha position of hydroxyl groups ($N_{H\alpha OH}$), as seen in Eq. (11). We could conclude that PLGA4 is terminated by 57 % of lactic acid, and 43 % of glycolic acid, with an average hydrogen on alpha of hydroxyl group of 1.43.

Average number of hydrogen bonds per OH group

$$= N_{H\alpha OH}\%_{LA} + N_{H\alpha OH}{}^{*}\%_{GA} \quad (11)$$

Those results led to the obtention an HEW value = 933 ± 14 g eq^{-1}, very close from the theoretical value (M_n divided by the functionality of PLGA4): HEW theoretical = 925 g eq^{-1}. Of notice, the agreement between the value of the experimental HEW, that is calculated using the chemical shifts of the PGLA chain ends, and of the value of the theoretical HEW, that is obtained from the monomer/initiator ratio, confirms that all hydroxyl groups have initiated a PLGA chain. This therefore allows us to consider that HEW corresponds to the molecular weight of each arm.

Regarding PLGA6 analysis, COSY analysis, seen in Fig. S3, helped us to attribute all signals of PLGA6. As seen in HSQC spectrum (see Fig. S4), the isolated marks of interest were attributed to $C_{c'}$ (66.8 ppm) and C_a (63 ppm). By integrating C_a as 6 carbons (as a reference for the core of the polymer) in quantitative ^{13}C (see Fig. S5), we could determine the integration of $C_{c'}$ at 3.5 carbons. This integration was confirmed with the one of $C_{d'}$ at 20.5 ppm, equal to 3.5 as well.

$H_{b'}$ was then obtained by subtracting 12 (H_a) and 3.5 ($H_{c'}$) to 18.7 (the integration of the signal gathering H_a, $H_{b'}$ and $H_{c'}$). In conclusion, $AH_{c'}$ = 3.5H and $AH_{b'}$ = 3.2H. PLGA6 was terminated by 64 % of LA and 36 % of GA, leading to an average hydrogen on alpha of the hydroxyl group of 1.36 H.

Those results led to the obtention of HEW value = 385 ± 6 g eq^{-1}, very close from the theoretical value (M_n divided by the functionality of PLGA6): HEW theoretical = 404 g eq^{-1}.

3.2. Poly(ester-urethane) synthesis and characterization

PEU obtained from linear PLGA-diol were thoroughly studied in our previous work [17,18]. For this reason, the present paragraph focuses on the two PEU series based either on PLGA4 or PLGA6. These series were prepared according to Table S3. The infrared spectra of the resulting PEU are provided in Fig. 2A for PEUs synthetized with PLGA4 and Fig. 2B for PEUs synthetized with PLGA6. A low-intensity peak in the absorption range of 3,360 to 3,320 cm^{-1} attributed to the amine –NH stretching vibration of a urethane bond appeared for all samples. The presence of the –CH_2 units in the polymer backbone is revealed by the set of peaks occurring between 2,940–2,930 cm^{-1} and 2,870–2,860 cm^{-1}. The absorption band around 2,230 cm^{-1} was notably missing from the majority of the infrared spectrum confirming that no free NCO group is left in the samples. However, this absorption band was still visible for PEU with the highest crosslinking percentage (PEU-15D) likely due to the challenges faced during the synthesis regarding the gelation point. Vibrations of the —C═O group of the PCL backbone, PLGA, and urethane bonds can be observed between 1,730–1,720 cm^{-1}.

As shown in Table 1, the samples exhibit conversion values ranging from 76 to 90 %. The lowest conversions reported are due to the anticipated stop of the polyaddition before the total conversion of isocyanates to avoid gelation. These lower conversions correspond to polyurethanes with high content of branching points resulting from high amounts of star PLGA and/or high number of arms (*eg.,* PEU-15D).

The molecular weights of the soluble fractions yield insightful information and were measured by SEC MALS. Analyses revealed an M_n of

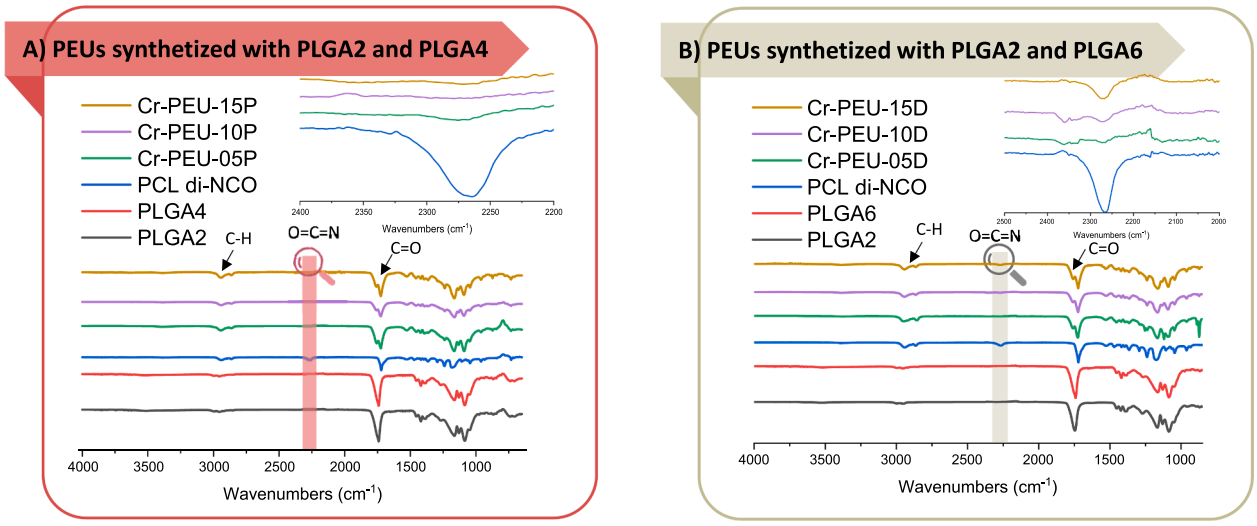

Fig. 2. FTIR Spectra of precursors and PEU based on A) PLGA4 and PLGA2, and B) PLGA6 and PLGA2.

Table 1
Isocyanate groups conversion, solubility and molecular weight of the PEU. NA means not applicable due to the insolubility of the PEUs.

Sample	Conversion (%)	Soluble (Yes/No)	M_n (g mol^{-1})	M_w (g mol^{-1})	Đ	GF (%)
Cr-PEU-05P	86.2	Yes	72,500	103,100	1.4	0
Cr-PEU-10P	87.8	Yes	53,700	127,200	2.4	0
Cr-PEU-15P	87.8	Yes	67,100	253,700	3.8	0
Cr-PEU-05D	81.2	Partly	NA	NA	NA	8
Cr-PEU-10D	80.0	Partly	NA	NA	NA	6
Cr-PEU-15D	76.1	Partly	NA	NA	NA	12
L-PEU	90.3	Yes	61,000	105,700	1.7	NA

30,600 g mol^{-1} for linear PEU and M_n ranging from 53,700 to 72,500 g mol^{-1} for PEU with PLGA4. Regarding the PEU containing PLGA6, due to a higher extent of crosslinking it was not possible to filter the samples for SEC analyses. Therefore, a gel fraction (GF) was calculated, ranging from 6 to 12 % which confirms the low extent of crosslinking that will enable further processing of the PEU, but that is high enough to hinder filtration for SEC analyses. Additionally, this GF gives us insights on the structure of our PEUs. Indeed, a high sol fraction reduces the density of elastically effective crosslinks, acting as voids within the material [19].

3.3. Poly(ester-urethane) thermal and mechanical properties

3.3.1. Poly(ester-urethane) thermal properties

The assessment of the thermal properties and thermal stability of polymers is of high importance to determine their potential domains of application and their processability. Therefore, these parameters were thoroughly investigated by DSC and TGA analyses, respectively. The DSC and TGA curves are shown in Fig. S6, while the melting temperatures (T_m) and onset thermal degradation temperature (T_d, 5 %) are gathered in Table S4.

All the obtained PEU possess quite similar melting points oscillating between 49 and 59 °C, and a glass transition at −60 °C (illustrating the glass transition of PCL blocks). For PEU synthetized with PLGA4, the T_m increased as the percentage of PLGA4 in the blend increased. However, this trend was not that clear for PEU synthetized with PLGA6, with T_m between 53 °C and 59 °C. Such finding could be mainly ascribed to different synthesis conditions such as the variations in the reaction time and the molecular weight of the polymer, among others. It was found that all the prepared materials exhibit high thermal stabilities over 200 °C, with onset decomposition temperatures (T_d, 5 %) appearing in the 220–265 °C range, leaving just 10 % and 5 % of residual weight upon heating to 400 °C and 600 °C, respectively. The demonstrated excellent resistance to heat ensures good thermal stability at temperatures much higher than the melting points of the synthesized PEU materials. This provides a broad thermal processing window up to 160 °C above respective T_m, thereby making the materials suitable candidates for hot-pressing. After conducting this study, thermocompression was conducted at 120 °C for 20 min under 1.2 tons of pressure to prepare the films studied in the rest of this work.

3.3.2. Poly(ester-urethane) tensile properties

The mechanical performance of the prepared PEUs is crucial for their practical uses. The mechanical properties of PEU films investigated by tensile testing are depicted in Fig. 3 and listed in Table 2. The developed PEU demonstrated a very wide range of stress–strain behaviours, ranging from hard (*e.g.,* Cr-PEU-10P and Cr-PEU-15D) to ductile (*e.g.,* Cr-PEU-05P, Cr-PEU-05D). The Young's moduli, tensile strength, and elongation at break were in the ranges of 5.86–96.3 MPa, 1.39–8.27 MPa, and 15–930 %, respectively, as seen in Table 2. As the percentage of PLGA4 and PLGA6 increased, the elongation at break decreased, as PLGA4 and PLGA6 act as crosslinking nods in the system bringing rigidity. Indeed, the density of urethane bonds is more important when the functionality of PLGA increases (at a constant molecular weight). However, an exception was found for Cr-PEU-15P which exhibits an elongation at break higher than excepted (930 % ± 32). The dispersity of 3.8 of this PEU underlines the inhomogeneity of the Cr-PEU-15P resulting by the high content of PLGA4 resulting in more branching and more chain extension as shown by its higher M_w compared to Cr-PEU-10P. Such mechanical performance could also be explained by the multiple interchain hydrogen-bonding interactions. The presence of ester groups in PCL and PLGA, combined to the expected higher density of urethane groups found locally when star PLGAs are used, enabled the formation of these physical interactions, which enhanced the overall mechanical strength of the materials. Moreover, the observed differences are possibly related to the orientation of the entanglement, which could be different in each sample. It's worth noting that the Young's modulus in the initial two series of synthesized PEUs (Fig. 3A and B) follows a consistent trend. At low PLGA star content, a lower Young's modulus was observed (55 MPa), which increased for 10 % of PLGA star,

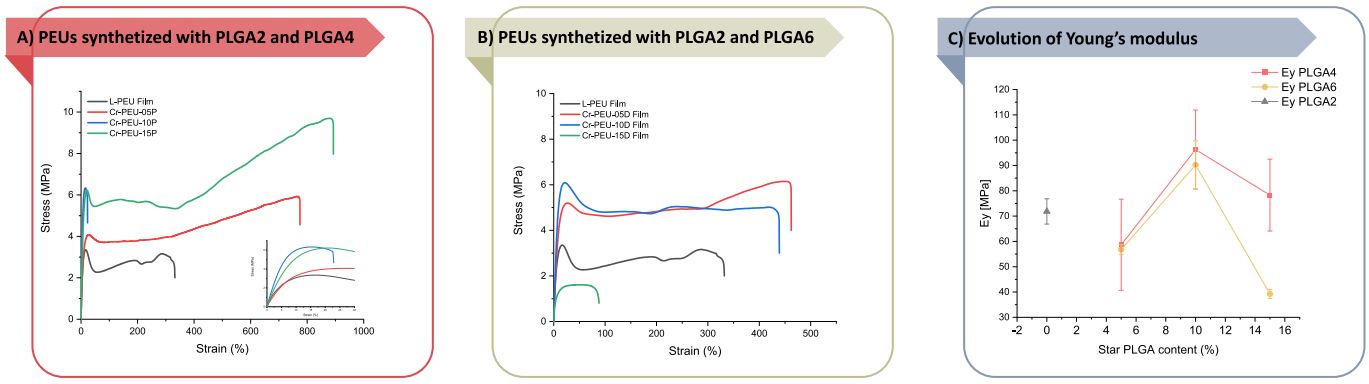

Fig. 3. Typical stress–strain curves of PEUs containing: A) PLGA4, B) PLGA6, and C) Evolution of Young's modulus as a function of PLGA content.

Table 2
Summary of tensile mechanical properties and of DMA characterizations of PEUS including shape memory properties with deformation ratios (R_d), fixity ratios (R_f) and recovery ratios (R_r).

	Tensile test			DMA			
PEU Films	Young's Modulus (E_Y) (MPa)	Tensile Strength (σ) (MPa)	Elongation at Break (ε) (%)	T_α (°C)	R_d (%)	R_f (%)	R_r (%)
Cr-PEU-05P	58.68 ± 18	5.73 ± 0.12	785 ± 28	29	53	89	92
Cr-PEU-10P	96.30 ± 15.60	4.76 ± 1.55	21.33 ± 4	42	NA	NA	NA
Cr-PEU-15P	78.29 ± 14.2	8.27 ± 0.19	930 ± 32	22	45	40	90
Cr-PEU-05D	56.76 ± 2.01	7.66 ± 1.5	728.33 ± 125	20	49	45	88
Cr-PEU-10D	90.26 ± 9.50	5.86 ± 0.44	266 ± 122	37	NA	NA	NA
Cr-PEU-15D	39.24 ± 1.78	1.54 ± 0.21	82 ± 6	48	NA	NA	NA
L-PEU	71.84 ± 5.06	3.9 ± 1.26	755 ± 220	29	60	45	88

to decrease again with 15 % of PLGA star. The Young's modulus decrease was even more pronounced for PLGA6, which exhibits more crosslinking nods than PLGA4, as seen in Fig. 3C.

This phenomenon was also observed in the work of Ahmad et al. [20] who investigated the influence of crosslinking/chain extension structure on mechanical properties of PU. They synthetized PU from IPDI and HTPB with two different crosslinking agents: 1,2,6-hexanetriol and trimethylolpropane and two different chain extenders: 1,4-butanediol and 1,6-hexanediol. A drop of ultimate elongation at break values after reaching a defined threshold of the triol/diol ratio was observed and indicated that an optimum crosslink density was reached, after which the rigid behaviour overtook the rubbery nature of the polymer.

3.3.3. *Poly(ester-urethane) shape memory properties*

After thoroughly characterizing the mechanical properties of the different PEUs, their shape memory properties were investigated. The T_α is usually obtained at the maximum of the loss modulus E'', however for our samples, the maximum was not clear and T_α of the different PEU films were obtained at the maximum of tanδ. The different Tα were found to be between 17 and 48 °C, as illustrated in Fig. S7.

Shape memory properties were evaluated on selected samples that were chosen based on their validation of the following parameters required to ensure efficient shape memory effect evaluation: i) a Tα 10 °C lower than actuation temperature fixed at 37 °C in our case), ii) a strain superior to 30 %, iii) a T_m 10 °C higher than T_α. As a consequence, the shape memory properties of Cr-PEU-10D were not tested due to its Tα of 37 °C. Sample Cr-PEU-10P was not evaluated due to its strain at break inferior to 22 %. Finally, samples Cr-PEU-10P and Cr-PEU-15D were also not tested as the Tα were not clear and could be possibly overlapped with their T_m. Indeed, at the end of the DMA program, when the temperature reached 60 °C, samples were melted. This observation clearly corelates with the drop of E' and E'' observed in Fig. S7C, F and G, and confirm the non-suitability of these two samples for shape memory effects.

For shape memory characterization, the samples were heated above the Tα, at 37 °C, to increase the chain mobility. Once the material was heated, a static force of 2 N was applied, before cooling to 10 °C to temporary fix the deformed shape. Then, the force was set to zero and the temperature was increased to 37 °C to activate the chain mobility and recover the sample's initial shape. A typical diagram illustrating the shape memory behaviour of L-PEU is provided in Fig. 4.

The diagrams illustrating the shape memory behaviour of the different PEU films can be seen in Fig. S8. The different PEU films exhibit a deformation ratio between 45 and 60 %, with the linear PEU exhibiting the highest deformation ratio of 60 % (see Table 2). Regarding the fixity ratios, the HS, hydrogen bonds, and crosslinking nods play a key role in determining the permanent shape of the structure. The fixity ratios were comprised between 40 and 89 %. Among PEU with star copolymers in their structure, the fixity ratio decreased as the number of crosslinking nods increased, a phenomenon that could be explained by a decrease in micro-phase separation. Cr-PEU-05P exhibited the highest fixity ratio of 89 %. Finally, recovery ratios were superior to 88 % that corresponds to the linear PEU with the highest value of 92 % reached with Cr-PEU-05P. Overall, we observed the improvement of shape memory properties for PEU synthetized with PLGA4 or PLGA6, compared to linear PU. Indeed, the degree of crosslinking within those systems is referred as net points that prevent switching segment chains from permanently sliding when a force is applied. They are acting as anchors that enable shape memory to occur [11]. The different values for R_d, R_f and R_r are in accordance with values of the literature, with PU synthetized with different isocyanates (HDI, IPDI) and alcohols (castor oil, PCL, PTMG) [4,6,7,9].

These results underline the good shape memory properties of PEU films such as shape fixity at an operating room temperature and fast shape recovery at physiological temperature.

To investigate in more details the possible applications of those PEUs, we aimed to process them as foams through a solvent casting/particulate leaching (SC/PL) process, where polymer solubility is essential. In a previous study, this process was investigated and optimised for linear poly(lactide-co-glycolide)/poly(ε-caprolactone) polyurethane [17]. To fabricate a foam, the previously synthesized PEU

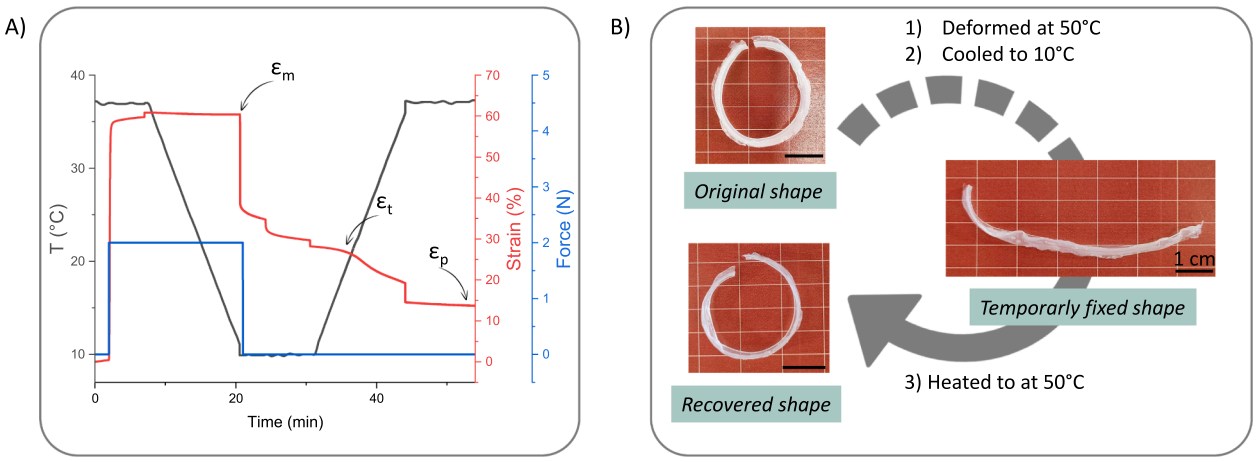

Fig. 4. Shape memory behaviour of L-PEU film. A) Typical conditions applied to evaluate the shape memory properties of the L-PEU sample and corresponding strains with maximum strain (ε_m), temporary shape (ε_t) and permanent shape recovered (ε_p). B) Photographs illustrating the shape memory behaviour of the L-PEU sample.

needs to be fully soluble in THF. The fully soluble PEUs (synthetized with PLGA4) were therefore investigated for foam engineering and fully characterized in term of porosity, pore size (SEM), and mechanical performance (compression test and DMA).

3.4. PEU-based foams

As mentioned in the previous section porous polymer foams were prepared by SC/PL with 15 g of NaCl salt as a porogen agent. 3 g of PEU was dissolved in 9 mL of THF for each sample. White foams were obtained after following the process described in the experimental part including steps of solvent evaporation and salt dissolution. The porosity of the foams was measured, and it was found to be in the range between 74 and 83 %. These values are suitable for cell proliferation and attachment and should be beneficial for regeneration of the meniscus [21]. The pore size was then evaluated using scanning electron microscopy images for two different foams: L-PEU foam and Cr-PEU-15P. SEM images show heterogeneous and interconnected porosity (Fig. 5). The pores size is different even if we used salt particles sized between 100 and 300 μm, which has been demonstrated as optimal for the ingrowth

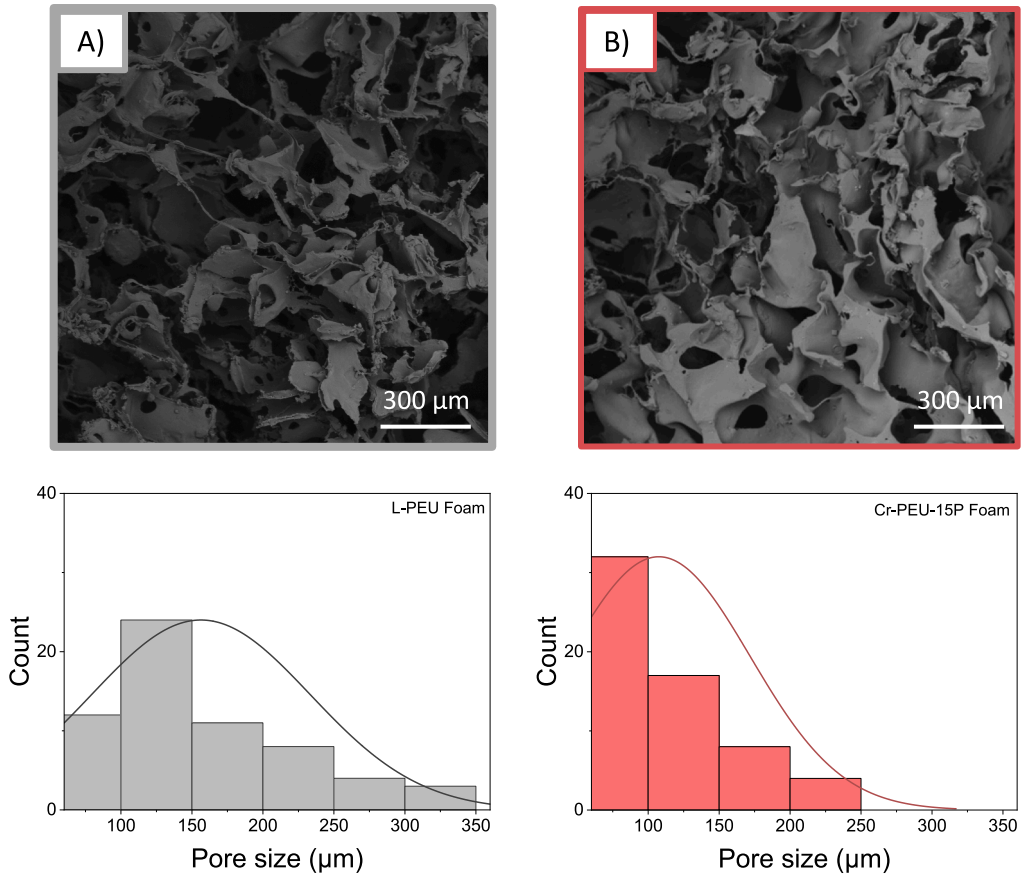

Fig. 5. SEM images and pore sizes distribution of A) L-PEU Foam and B) Cr-PEU-15P Foam.

of fibrocartilaginous tissue. The linear PEU foam shows one large population of pores between 100–150 μm, with an average pores size of 156 ± 35 μm. For Cr-PU-15P foam, the average pores size was lower with a mean value at 110 ± 75 μm.

The mechanical properties of the different foams were investigated. Compression tests at 20 % compression were performed at room temperature. Increasing the ratio of PLGA star in the foam did not have a strong impact on Young's modulus with E_y values of 0.22, 0.32, 0.15 MPa for Cr-PEU-05P, Cr-PEU-10P and Cr-PEU-15P foams, respectively. These values were slightly higher than the one obtained from linear PEU ($E_y = 0.13 \pm 0.09$ MPa) and are all close to the ones reported for human meniscus (around 0.15 MPa [22], 0.24 MPa [23], and 0,67 MPa [24]).

Dynamic mechanical analyses were performed to investigate the viscoelastic properties at 1 Hz of the PEU containing linear PLGA2 or star PLGA4. Fig. 6B and Fig. 6C show the storage modulus (E') and tan (δ) measurements between 15 °C and 45 °C.

At room temperature, a limited increase of storage modulus is observed for PEU polymers synthetized with PLGA4, showing a maximum of 15 % increase from 1.75 MPa to around 2.01 MPa, for L-PEU and Cr-PEU-10P, respectively (Table 3). At 37 °C, PLGA4-based PEU witnessed an increase of storage modulus with the content of star PLGA4 with up to 40 % higher values for Cr-PEU-15P compared to the L-PEU control. At this physiological temperature, all foams fall within the accepted range (storage modulus between 0.42 MPa and 0.77 MPa) for meniscal repair. All T_α values are close with values ranging between 33 and 35 °C.

The flexibility of the foams was also tested. The different foams were subjected to a 3-point bending test at 100 % flexion to mimic the movements performed by surgeons during surgeries, as illustrated in Fig. 7. The linear L-PEU foam was less flexible than Cr-PEU-15P. A higher force was necessary to reach 90 % of flexion for the L-PEU foam with a flexural strength of 1.04 ± 0.03 MPa compared to as low as 0.25 ± 0.01 MPa for Cr-PEU-15P. This 4-folds decrease could be explained by the crosslinking nods in the Cr-PEU-15P structures, brought by PLGA star.

Flexural strength is controlled by a complex interplay between glass transition temperature, type and density of crosslinks (covalent vs. physical), dynamic of the physical-crosslinks (H-bonds), and the phase separation occurring between HS and SS in the polymer. In particular, HS domains (structure, order, concentration) play a very important role on the final structure, morphology, and properties PU foams [25]. It is our belief that upon addition of star PLGA4 in the PEU, the covalent nods hinder the formation of phase separated hard-domains leading to lower T_a (22 °C for Cr-PEU-15P vs. 29 °C for L-PEU, see Table S4) and lower flexural strength. This is reported by Thomas et al. who studied the effect of increasing the crosslink density on the morphology of flexible polyurethane foams and demonstrated that increasing the polyol functionality increased the phase mixing [26]. Of notice, in our case, upon addition of same amounts of star PLGA6, the higher covalent crosslinking density increases this same T_a (48 °C for Cr-PEU-15P) and hinder foam preparation of the resulting insoluble PEU.

This improved flexibility was positively evaluated by an experienced orthopedic surgeon (M.A.) and holds potential for mini-invasive surgery applications.

Table 3
Summary of mechanical characteristics and porosity of foams synthetised with different amount of star PLGA4.

PEU Foams	Porosity (%)	E_y (MPa)	E' (25 °C) (MPa)	E' (37 °C) (MPa)	T_α (°C)
Cr-PEU-05P	83 ± 1	0.22 ± 0.03	1.76	0.42	34
Cr-PEU-10P	78 ± 3	0.32 ± 0.11	2.01	0.60	33
Cr-PEU-15P	81 ± 1	0.15 ± 0.06	1.86	0.77	35
L-PEU	74 ± 4	0.13 ± 0.09	1.75	0.55	33

3.5. Degradation

A degradation study was performed in PBS at 37 °C to evaluate the influence of PLGA4 on the evolution of residual mass over time. The L-PEU and Cr-PEU-15P foams, were compared, as seen in Fig. 8. For both foams, after 6 weeks of incubation, it was difficult to weight the samples as they were falling apart. Cr-PEU foam is degrading slightly faster than L-PEU with a remaining mass of 60 % for Cr-PEU-15P and 69 % for L-PEU foam after 6 weeks immersed in PBS. In more details, Cr-PEU-15P showed steady mass loss from the start of the degradation study, whereas a lag time up to 3 weeks was witnessed for L-PEU. These different profiles are typical of degradable thermoplastics vs. degradable crosslinked polymers the latter being known to exhibit linear mass loss profiles [27]. In our case, PLGA4 hydrolysis leads to water-soluble oligomers much more rapidly than their linear PLGA counterparts due to the low molecular weights of the initial arms (ca. 900 g/mol vs. 1900 g/mol for linear PLGA). At a same hydrolysis rate, the statistical cleavage of ester groups in the arms of PLGA4 yields more rapidly short water-soluble oligomers able to diffuse out of the polymer matrix rapidly after the initiation of the degradation study.

4. Conclusions

Two series of polyester-urethane (PEU) were obtained from linear and star-shaped PLGA polyols initiated by pentaerythritol, or dipentaerythritol and reacted with PCL di-NCO prepolymer. The resulting

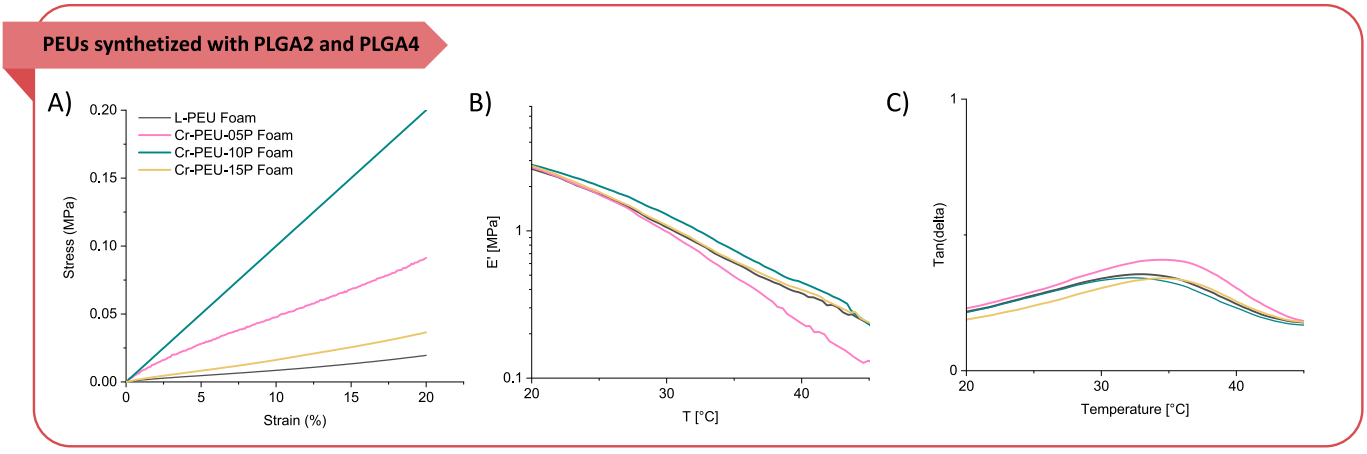

Fig. 6. Mechanical analyses of PEU foams: A) Stress strain compression curve at 20% of compression of PEU foams synthetized with PLGA4, B), E' in the function of the temperature of PEU foams synthetized with PLGA4 and C) Tan(δ) of PEU foams synthetized with PLGA4.

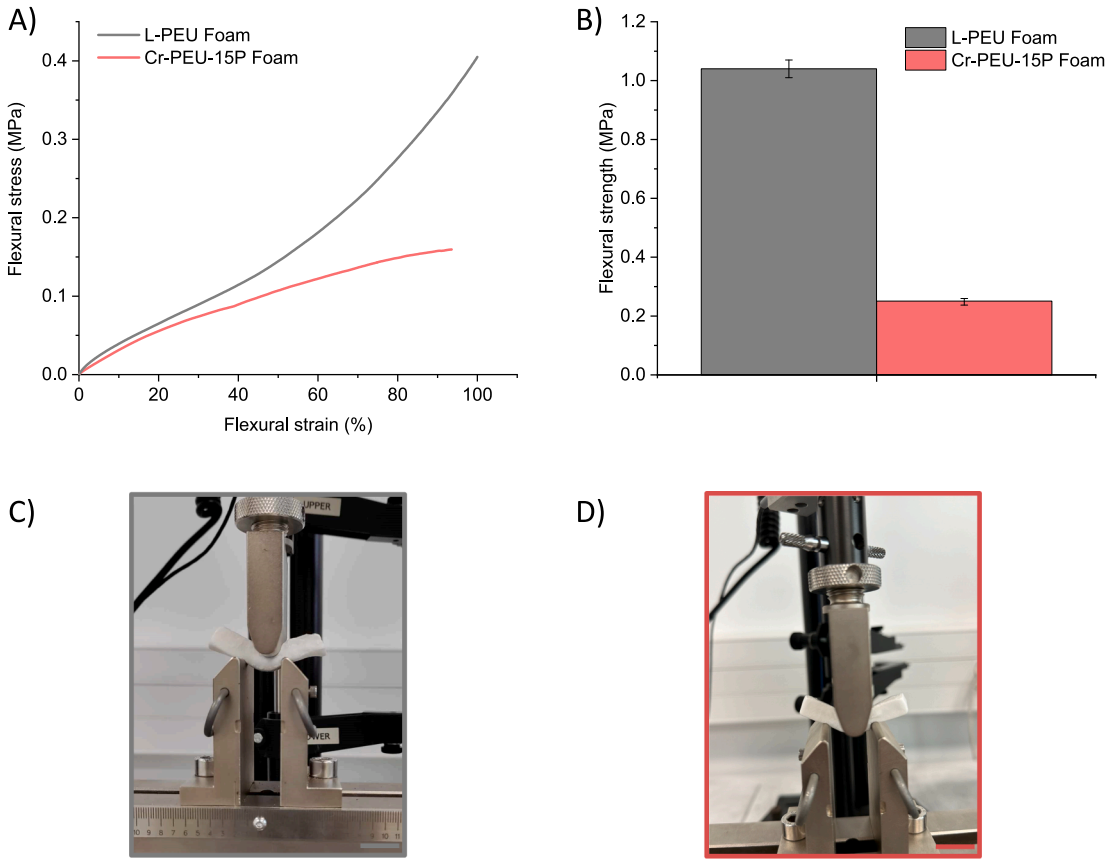

Fig. 7. Flexion test of foams prepared with L-PEU and Cr-PEU-15P. A) Flexural stress strain curve at 90 % flexion. B) Flexural strength of foams. C),D) Macrographs at 90 % of flexion of foams prepared with L-PEU and Cr-PEU-15P, respectively.

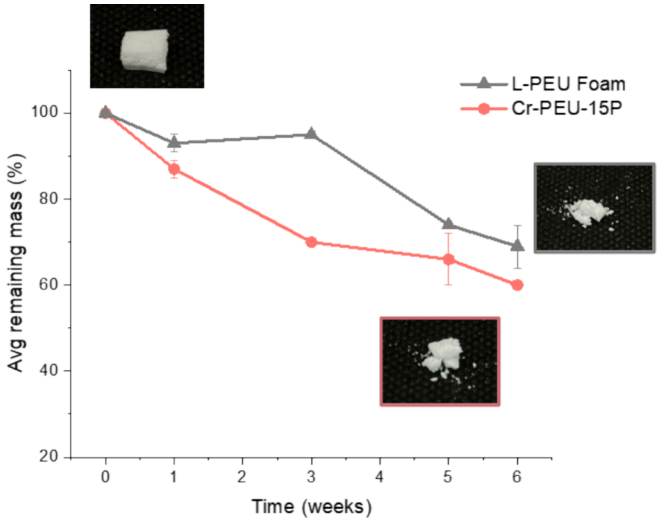

Fig. 8. Degradation study (PBS, 37 °C, pH=7.4) of PEU foams. Evolution of residual mass over time with pictures of the foams at day 0 and week 6 for L-PEU and Cr-PEU-15P foams.

PEUs' mechanical properties were evaluated. The films exhibited large range of mechanical properties, with a Young's modulus of up to 96 MPa, a high elongation at break of 930 %. Moreover, we showed that incorporating PLGA star within the PEU structure could enhance the shape memory ability. The fixity ratio is increased from 79 % to 96 % while the recovery ratio is increased from 87 % to 92 % when comparing L-PEU with Cr-PEU-15P. To dig further into the possible applications of those shape memory PEU, the solvent casting/particles leaching (SC/PL) process was used to formulate porous foams that were fully thermally and mechanically characterized. High porosity within the range of 74 % to 83 %, pore size ranging from 100 to 300 μm, and mechanical properties that closely align with the human meniscus (Young's modulus ranging from 0.13 MPa to 0.53 MPa). The foam prepared from star PLGA4 exhibit a better flexibility than linear PEU foam with a flexural strength of 1.04 ± 0.03 MPa for L-PEU foam and 0.25 ± 0.01 MPa for Cr-PEU-15P). In summary, biodegradable PEU materials based on star polyesters were designed, exhibiting shape memory properties as film and enhanced flexibility as scaffolds which makes them good candidate for biomedical applications.

CRediT authorship contribution statement

Gaëlle Savin: Writing – original draft, Methodology, Investigation. **Iliass Kadmiri:** Investigation. **Sylvain Caillol:** Writing – review & editing, Supervision. **Philippe Gonzales:** Investigation. **Aurélien Lebrun:** Methodology, Investigation. **Michel Assor:** Project administration, Funding acquisition. **Ghislain David:** Writing – review & editing, Supervision, Project administration, Methodology, Funding acquisition, Conceptualization. **Benjamin Nottelet:** Writing – review & editing, Supervision, Project administration, Methodology, Funding acquisition, Conceptualization.

Declaration of competing interest

The authors declare the following financial interests/personal relationships which may be considered as potential competing interests: Gaelle Savin reports financial support was provided by Arthorcart Biotech. Michel Assor reports a relationship with Arthorcart Biotech that

includes: board membership. Ghislain David reports a relationship with Arthorcart Biotech that includes: board membership. no conflict of interest to disclose If there are other authors, they declare that they have no known competing financial interests or personal relationships that could have appeared to influence the work reported in this paper.

Data availability

Data will be made available on request.

Acknowledgements

This work was supported and funded by Arthrocart Biotech and by ANRT (2020-1381). Authors thank Vincent Darcos for the analyses carried out on the Synbio3 platform.

Appendix A. Supplementary data

Supplementary data to this article can be found online at https://doi.org/10.1016/j.eurpolymj.2024.113442.

References

[1] A. Lendlein, M. Behl, B. Hiebl, C. Wischke, Expert Rev Med Devices 7 (2010) 357–379.
[2] J. Delaey, P. Dubruel, S. Van Vlierberghe, Adv Funct Mater 30 (2020) 1909047.
[3] D.L. Safranski, K. Gall, Polymer 49 (2008) 4446–4455.
[4] S.H. Baek, J.H. Kim, Polym Test 103 (2021) 107366.
[5] A. Nissenbaum, I. Greenfeld, H.D. Wagner, Polymer 190 (2020) 122226.
[6] W. Zhao, L. Liu, F. Zhang, J. Leng, Y. Liu, Mater Sci Eng C 97 (2019) 864–883.
[7] A. Shaabani, R. Sedghi, Polymer 223 (2021) 123694.
[8] M. Ramezani, M.B.B. Monroe, ACS Appl Polym Mater 4 (2022) 1956–1965.
[9] A. Veloso-Fernández, J.M. Laza, L. Ruiz-Rubio, A. Martín, M. Taguado, A. Benito-Vicente, C. Martín, J.L. Vilas, Mater Today Commun 33 (2022) 104730.
[10] K. Hearon, M.A. Wierzbicki, L.D. Nash, T.L. Landsman, C. Laramy, A.T. Lonnecker, M.C. Gibbons, S. Ur, K.O. Cardinal, T.S. Wilson, K.L. Wooley, D.J. Maitland, Adv Healthc Mater 4 (2015) 1386–1398.
[11] A. Lendlein, S. Kelch, Shape-memory polymers, Angew Chem Int Ed Engl 41 (2002) 2035–2057.
[12] Z. Miri, S. Farè, Q. Ma, H.J. Haugen, Prog Biomed Eng 5 (2023) 042001.
[13] Q. Luo, J. Chen, P. Gnanasekar, X. Ma, D. Qin, H. Na, J. Zhu, N. Yan, New J Chem 44 (2020) 658–662.
[14] W. Yang, W. Yang, D. Guan, J. Liu, Y. Luo, Y. Wang, D. Guan, J. Liu, Y. Luo, Y. Wang, New J Chem 44 (2020) 3493–3503.
[15] M. Bil, E. Kijeńska-Gawrońska, E. Głodkowska-Mrówka, A. Manda-Handzlik, P. Mrówka, Mater Sci Eng C 110 (2020) 110675.
[16] S.M. Hong, J.Y. Yoon, J.R. Cha, J. Ahn, N. Mandakhbayar, J.H. Park, J. Im, G. Jin, M.Y. Kim, J.C. Knowles, H.H. Lee, J.H. Lee, H.W. Kim, Bioeng Transl Med 7 (2022) e10332.
[17] G. Savin, O. Sastourne-Array, S. Caillol, A. Bethry, M. Assor, G. David, B. Nottelet, Molecules 29 (2024) 766.
[18] G. Savin, S. Caillol, A. Bethry, E. Rondet, M. Assor, G. David, B. Nottelet, Biomater Sci 12 (2024) 2960–2977.
[19] C. W. H. Rajawasam, O. J. Dodo, M. A. S. N. Weerasinghe, I. Raji, S. Wanasinghe, D. Konkolewicz and N. De Alwis Watuthanthrige, *Polym Chem*, 2024, 15, 219-247.
[20] N. Ahmad, M.B. Khan, X. Ma, N. Ul-Haq, Arab J Sci Eng 39 (2014) 43–51.
[21] R. Al Nakib, A. Toncheva, V. Fontaine, J. Vanheuverzwijn, J. M. Raquez and F. Meyer, *J Appl Polym Sci*, 2022, **139**, 51666.
[22] A. Abdelgaied, M. Stanley, M. Galfe, H. Berry, E. Ingham, J. Fisher, J Biomech 48 (2015) 1389–1396.
[23] M.A. Sweigart, C.F. Zhu, D.M. Burt, P.D. Deholl, C.M. Agrawal, T.O. Clanton, K. A. Athanasiou, Ann Biomed Eng 32 (2004) 1569–1579.
[24] H.N. Chia, M.L. Hull, J Orthop Res 26 (2008) 951–956.
[25] L. Valette, C.-P. Hsu, Polymer 40 (1999) 2059–2070.
[26] H.C. Jung, S.C. Ryu, W.N. Kim, Y.-B. Lee, K.H. Choe, S.-B. Kim, J Appl Polym Sci 81 (2001) 486–493.
[27] M. Grosjean, S. Ouedraogo, S. Déjean, X. Garric, V. Luchnikov, A. Ponche, N. Mathieu, K. Anselme, B. Nottelet, ACS Appl Mater Interfaces 14 (2022) 43719–43731.